Effect of hysteresis on water flow in a sand column with a fluctuating capillary fringe

Peter Lehmann [a,*], Fritz Stauffer [b,1], Christoph Hinz [a,c],
Olivier Dury [a], Hannes Flühler [a]

[a] *Institute of Terrestrial Ecology, Swiss Federal Institute of Technology, ETH Zurich, CH-8952 Schlieren, Switzerland*
[b] *Institute of Hydromechanics and Water Resources Management, ETH Zurich, CH-8093 Zurich Hoenggerberg, Switzerland*
[c] *Institute of Soil Science and Forest Nutrition, University of Göttingen, D-37077 Göttingen , Germany*

Abstract

The transport of water and solutes from the topsoil to groundwater is sensitive to the mixing regime near and within the capillary fringe. The capillary fringe is the transition zone between the saturated and unsaturated regions of the vadose zone. This study was conducted to describe variations of water content and matric potential in the presence of a capillary fringe. We used a sand column with a fluctuating water table to explore the dynamics of the phase distributions. A column 57 cm in length and 5.3 cm in diameter was packed with a sand mixture. The water pressure fluctuated at the bottom and forced the capillary fringe to move within the column. The column was installed on a balance for measuring the total water mass in it. Water content and potential were measured at different soil depths using TDR probes and tensiometers. The first series of experiments was conducted without irrigating. In a second series water was added to the surface at a constant rate by means of a sprinkling system. The variations of water content and matric potential were increasingly dampened and shifted in time with increasing distance from the capillary fringe. To describe the dynamics of water distribution it was necessary to account for hysteresis. Hysteresis dampened the water dynamics and caused a highly asymmetrical response of water content to the symmetrically oscillating lower boundary condition. The water dynamics were simulated with the computer code HYSTFLOW [Stauffer, F., 1996. Hysteretic unsaturated flow modelling. In: Proceedings of the Second International Conference on Hydroinformatics, Hydroinformatics '96, Zürich, Switzerland. Balkema, Rotterdam, pp. 589–595] which is based on Richards' equation, the Brooks and Corey hydraulic functions and a modified Mualem [Mualem, Y., 1984. A modified dependent-domain theory of hysteresis. Soil Sci. 137 (5), 283–291]

---

* Corresponding author. E-mail: lehmann@ito.umnw.ethz.ch
1 Also corresponding author. E-mail: stauffer@ihw.baum.ethz.ch

hysteresis model. The water dynamics including the hysteretic behaviour were well described by the simulations. © 1998 Elsevier Science B.V. All rights reserved.

1. Introduction

This study is part of a multidisciplinary project focussed on transport of organic pollutants in the unsaturated zone. The description of water flow and phase distribution is the basis for understanding the transport of dissolved organic pollutants from soil surface to groundwater. The fate of organic chemicals does not only depend on its interactions with the solid phase, but also on the water flow velocity in the soil. Water flow largely depends on the amount and intensity of precipitation and evapotranspiration, as well as by the movement of the free water table in the subsoil or the aquifer. Drying and wetting processes driven by water potential differences may occur simultaneously at different depths under field conditions. Therefore the governing flow equations for water in soils has to account for the water-content changes induced by changes in water potential. While the influence of the gravitational potential on the amount of water is identical for drying and wetting processes, the relationship between matric potential and water content may depend on wetting and drying history (Hillel, 1980). For a given matric potential the water content may vary within wide limits. This effect of a non-unique water-retention curve, the soil water hysteresis, is relevant for the gas-phase continuity within or near the capillary fringe.

In a coarse sand the height of the capillary fringe is much larger during a drying than a wetting cycle. In the zone of varying extensions of the capillary fringe, the water content, pore water velocity and hydraulic conductivity change according to saturation. These variations modify the water, solute and gas transport from the soil surface to the aquifer (Russo et al., 1989). They affect the water content profile which in turn influences aeration and hence various chemical and microbial processes.

The hysteresis phenomenon has been well documented in the literature beginning with the work of Haines (1930). In several experimental studies soil water hysteresis was investigated during full drying and wetting steps allowing sufficient equilibration time between steps (Philip, 1964; Poulovassilis and Childs, 1971). In natural systems, however, cyclic boundary conditions are more common than discrete drying or wetting steps. Hysteresis effects on water flow driven by a cyclic upper boundary condition was investigated by Jaynes (1992). Numerical and analytical studies with fluctuating lower boundary conditions were conducted by Raats and Gardner (1974) and Hinz (1998) without taking into accounthysteresis. Stauffer (1996) calculated the influence of hysteresis on the response of water content and pressure profiles in a sand column to a fluctuating water table using a modified Mualem (1984) hysteresis model. Hoa et al. (1977) carried out column experiments with a fluctuating lower pressure boundary and simulated the experiment with an empirical hysteretic water-retention curve.

Our study expands on the above work by including the influence of oscillation frequency, initial state and input flux at the upper boundary. We analyse the effect of

hysteresis on water storage, water content and the pressure profile in a sand column subjected to fluctuating pressure conditions at the lower boundary. The dynamics of the boundary conditions in natural systems are idealised as a triangular wave function of the pressure at the lower boundary. This causes alternating hysteretic wetting and drying processes. We expected dampened fluctuations delayed in time with increasing distance from the lower boundary due to a decreasing hydraulic conductivity in the unsaturated zone. Therefore the zone within and above the capillary fringe should exhibit the highest and fastest response and contribute most to the changes of total water mass.

In the quasi-saturated zone of the capillary fringe the air pressure may not be continuous and the validity of Richards' equation is therefore possibly limited. To avoid this difficulty, three-dimensional pore network models were developed by Reeves and Celia (1996) to simulate hysteresis and by Blunt and Scher (1995) to describe water and air flow near the capillary fringe. However, these models are still limited to small scales and not applicable at the column scale. Therefore the Richards equation was used to describe the water dynamics in our sand column under unsaturated conditions. This study is thus also relevant to the discussion about the validity of Richards' equation to describe water transport in the unsaturated zone of a sand under different boundary conditions.

2. Theory

2.1. Water transport

One-dimensional unsaturated water flow is described by the Richards equation

$$C_{\mathrm{W}}(\psi)\frac{\partial \psi}{\partial t} = \frac{\partial \psi}{\partial z}\left[K(\theta)\left(1 + \frac{\partial \psi}{\partial z}\right)\right] \tag{1}$$

with the vertical coordinate z (cm) being positive in the upward direction, the matric potential head ψ (cm), which is negative for unsaturated soil, the hydraulic conductivity $K(\theta)$ (cm min^{-1}) depending on the volumetric water content θ (cm^3 cm^{-3}) and the specific water capacity $C_{\mathrm{W}}(\psi)$ (cm^{-1}) defined as

$$C_{\mathrm{W}}(\psi) = \frac{\partial \theta}{\partial \psi} \tag{2}$$

which shows itself a strongly hysteretic dependence on ψ because it is the derivative of the hysteretic water-retention function. For the water-retention curve and the hydraulic conductivity function of the sand we used the Brooks and Corey model (Brooks and Corey, 1966).

The water retention function is

$$\frac{\theta - \theta_{\mathrm{r}}}{\phi - \theta_{\mathrm{r}}} = \left(\frac{-\psi_{\mathrm{CF}}}{-\psi}\right)^{\lambda} \tag{3}$$

with $-\psi_{CF}$ being the height of the capillary fringe (air entry value) in cm with different values for wetting or drying processes, the porosity ϕ (cm^3 cm^{-3}), the residual water content θ_r (cm^3 cm^{-3}) and the curve shape parameter λ (−).

The corresponding function for the unsaturated hydraulic conductivity $K_u(\theta)$ (cm min^{-1}) is estimated as

$$K_u(\theta) = K_s(\phi)\left(\frac{\theta - \theta_r}{\phi - \theta_r}\right)^{3 + \frac{2}{\lambda}} \tag{4}$$

where $K_s(\phi)$ (cm min^{-1}) is the conductivity under completely saturated conditions. It is important to note that the conductivity is here defined as a function of θ and is assumed to be nonhysteretic.

2.2. Theory of hysteretic water-retention function

In order to describe the hysteretic behaviour of a particular soil, many wetting and drying experiments have to be performed, because the water-retention function may change with each drying and wetting process. Such measurements are extremely time-consuming and delicate to carry out. Therefore a theory is needed to estimate the water-retention function for any drying and wetting loop based on the envelope of main drying and wetting curves. The main drying curve describes the drying from the highest reproducible saturation degree, which is usually not complete due to entrapped air, to the residual water saturation. The main wetting curve describes the wetting from the residual water content to the highest saturation degree. Starting from a boundary wetting or drying curve, a sequence of wetting and drying cycles can be expressed by scanning curves (primary, secondary or higher order).

Two main groups of hysteresis models are found in the literature (Jaynes, 1992). The first group describes the scanning curves with expressions similar to the main drying and wetting curves, assuming the same curve shape parameters (Kool and Parker, 1987, among others). The second group explains the shape of the scanning curves by means of physical properties such as the distribution of the pore radii (Mualem, 1973, among others). This latter approach is also useful for describing solute transport under unsaturated conditions, because sorption processes as well as velocity distributions may depend on the pore radii variation (Sugita and Gillham, 1995a,b; Sugita et al., 1995; Durner and Flühler, 1996). Our study uses a hysteretic model of this second type and is based on the model of Mualem (1984).

The hysteresis effect is caused by different controlling pore radii and contact angles for wetting and drying processes. In the following the effect of varying contact angles is neglected. Each pore is characterized by an opening radius r and a body radius ρ. When the water potential head Ψ exceeds the wetting threshold value Ψ_w depending on ρ, the pore becomes filled. When the matric potential falls again below this value, the pore only drains if the opening radius r is not smaller than the body radius ρ. If $\rho > r$, the pore does not drain until the potential is decreased to the drying threshold value Ψ_d, determined by r. For the case $\rho \leq r$, the pore drains and rewets at the same potential value $\Psi_w = \Psi_d$. In this case wetting and drying processes are reversible.

This argumentation is a physical illustration of the hysteresis model of Mualem (1974). Conceptually it is an independent-domain model, where the pore space is assumed to be divided into a series of independent subdomains (in this simplified illustration described as pores), characterized by the radii ρ and r. The pore volume distribution function $f(r,\rho)$ is assumed to be a product of two independent functions, the pore opening radii distribution $g(r)$ and the pore body radii distribution $l(\rho)$

$$f(\rho,r) = l(\rho)\, g(r). \tag{5}$$

Mualem (1977) postulated that $g(r)$ and $l(\rho)$ represent areal and volumetric pore distributions. In this case the two distribution functions g and l are assumed to be identical which yields a function with only one unknown variable g

$$f(\rho,r) = g(\rho)\, g(r). \tag{6}$$

The (measured) water content corresponds to an integration over the pore volume distribution function. The integration is based on the different limiting opening and body radii for each wetting and drying process. This is explained and illustrated with Mualems' pore diagrams in Mualem (1974). The prediction of the scanning curves with this model is poor, if a major portion of the hysteresis loop lies in the matric potential range above the air entry value of the main drying curve (Mualem and Dagan, 1975). This deficiency is attributed to a blockage against entry of air to some pores because of their dependence on the state of neighboring pores. This may be the case for pores embedded within the soil, where air cannot penetrate until the surrounding pores have drained (Jaynes, 1992). Mualem and Dagan (1975) and Mualem (1984) formulated a dependent-domain model, taking into account a weighting-function $P_d\{\theta\} \leq 1$, which represents the ratio between the drained volume of dependent and independent pores with free access to air entry. The inverse effect of air blockage against water entry under highly unsaturated conditions is neglected. Stauffer (1996) modified the calculation of the weighting function to simplify numerical modeling. In the following, results and equations are summarised.

In Mualem (1984) the weighting function is given as a function of the main wetting and main drying curves

$$P_d\{\theta\} = (\theta_u - \theta_r)\frac{\left[\theta_u - \theta_d(\Psi)\right]}{\left[\theta_u - \theta_w(\Psi)\right]^2} \tag{7}$$

with the main drying curve $\theta_d(\psi)$, the main wetting curve $\theta_w(\psi)$, the reproducible maximum water content θ_u, called 'satiated' water content (Mualem and Miller, 1979) and the residual water content θ_r. To calculate the unknown water content $\theta(\psi)$ after several drying and wetting processes, the value of the weighting-function must be known. Since this value depends also on the unknown water content $\theta(\psi)$, for drying processes the water content cannot be expressed as an explicit function. Stauffer (1996) modified Mualem's concept and used $P_d\{\theta_d(\psi)\}$ as an approximation for $P_d\{\theta(\psi)\}$ to define an explicit function for the unknown water content. He took the value of the weighting-function that corresponds to the water content on the main drying curve with the same matric potential.
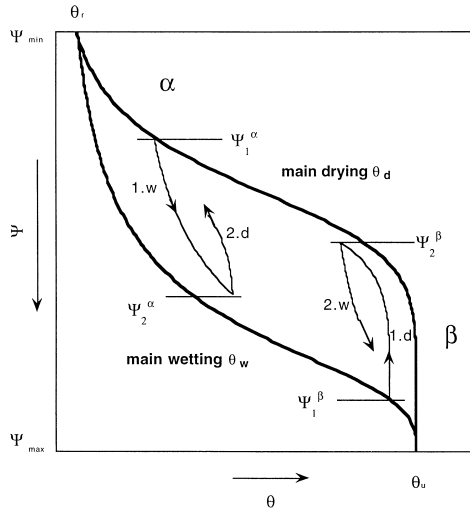
Fig. 1. Hysteresis of water retention curve. Examples of scanning curves calculated by Eqs. (9)–(12).

In Fig. 1 two calculated pairs of scanning curves using the approximation of Stauffer (1996) are shown for illustration. The water content on the primary wetting scanning curve (1.w) in example α is according to Mualem (1984)

$$\theta \begin{pmatrix} \Psi_{max} & & \Psi \\ & \Psi_1^\alpha & \end{pmatrix}$$

$$= \theta_d(\Psi_1^\alpha) + \frac{P_d\{\theta_d(\psi_1^\alpha)\}}{(\theta_u - \theta_r)} [\theta_u - \theta_w(\Psi_1^\alpha)][\theta_w(\Psi) - \theta_w(\Psi_1^\alpha)] \qquad (8)$$

with Enderby's notation (Enderby, 1955) of the complete drying and wetting history. In this case Ψ decreases from Ψ_{max} to Ψ_1^α and is increased again from Ψ_1^α to Ψ. Note that the weighting-function of the most recent drying process has to be used (Topp, 1971). Here it is the value $P_d\{\theta_d(\psi_1^\alpha)\}$ at the endpoint of the preceding drying process. Inserted in Eq. (8) it yields

$$\theta \begin{pmatrix} \Psi_{max} & & \Psi \\ & \Psi_1^\alpha & \end{pmatrix} = \theta_d(\Psi_1^\alpha) + \frac{[\theta_u - \theta_d(\Psi_1^\alpha)]}{[\theta_u - \theta_w(\Psi_1^\alpha)]} [\theta_w(\Psi) - \theta_w(\Psi_1^\alpha)]. \qquad (9)$$

The water content on the following secondary drying scanning curve (2.d) is

$$\theta \begin{pmatrix} \Psi_{max} & & \Psi_2^\alpha & \\ & \Psi_1^\alpha & & \Psi \end{pmatrix} \approx \theta \begin{pmatrix} \Psi_{max} & & \Psi_2^\alpha \\ & \Psi_1^\alpha & \end{pmatrix}$$

$$- \frac{[\theta_u - \theta_d(\Psi)]}{[\theta_u - \theta_w(\Psi)]} [\theta_w(\Psi_2^\alpha) - \theta_w(\Psi)] \qquad (10)$$

In example β of Fig. 1 the potential is increased from Ψ_{min} to Ψ_1^β, then decreased to

Ψ_2^{β} and increased again. The water content on the primary drying scanning curve (1.d) is approximated by

$$\theta\left(\begin{matrix} & \Psi_1^{\beta} & \\ \Psi_{\min} & & \Psi \end{matrix}\right) \approx \theta_w(\Psi_1^{\beta}) - \frac{[\theta_u - \theta_d(\Psi)]}{[\theta_u - \theta_w(\Psi)]}[\theta_w(\Psi_1^{\beta}) - \theta_w(\Psi)] \quad (11)$$

and on the following secondary wetting scanning curve (2.w) by

$$\theta\left(\begin{matrix} & \Psi_1^{\beta} & & \Psi & \\ \Psi_{\min} & & \Psi_2^{\beta} & & \end{matrix}\right) \approx \theta_d\left(\begin{matrix} & \Psi_1^{\beta} & & \\ \Psi_{\min} & & \Psi_2^{\beta} & \end{matrix}\right)$$
$$+ \frac{[\theta_u - \theta_d(\Psi_2^{\beta})]}{[\theta_u - \theta_w(\Psi_2^{\beta})]}[\theta_w(\Psi) - \theta_w(\Psi_2^{\beta})]. \quad (12)$$

All equations for scanning curves of higher order are approximated by Stauffer (1996) along the lines of Mualem (1984), so that any hysteretic loop can be calculated explicitly: Drying scanning curve of order n

$$\theta_{n,d}\left(\begin{matrix} \cdots & \Psi_{n-1} & \\ \cdots & \cdots & \Psi \end{matrix}\right) \approx \theta_{n-1,w}\left(\begin{matrix} \cdots & & \Psi_{n-1} \\ \cdots & \Psi_{n-2} & \end{matrix}\right)$$
$$- \frac{[\theta_u - \theta_d(\Psi)]}{[\theta_u - \theta_w(\Psi)]}[\theta_w(\Psi_{n-1}) - \theta_w(\Psi)] \quad (13)$$

and wetting scanning curve of order n

$$\theta_{n,w}\left(\begin{matrix} \cdots & & \Psi \\ \cdots & \Psi_{n-1} & \end{matrix}\right) \approx \theta_{n-1,d}\left(\begin{matrix} \cdots & \Psi_{n-2} & \\ \cdots & & \Psi_{n-1} \end{matrix}\right)$$
$$+ \frac{[\theta_u - \theta_d(\Psi_{n-1})]}{[\theta_u - \theta_w(\Psi_{n-1})]}[\theta_w(\Psi) - \theta_w(\Psi_{n-1})]. \quad (14)$$

The uncertainty of these approximations increases with each step, since each equation is composed of the approximated previous state and the estimation of the actual water content changing. It is important to investigate the validity of this approximation with experimental results.

3. Materials and methods

3.1. Experimental system

The experiments were performed with a packed sand column. Characteristics of the column system are summarised in Table 1. The transparent PVC column had a length of 57 cm and an inner diameter of 5.3 cm. The particle size of the quartz sand ranged from 80 to 1250 μm. The small sand fraction (80 to 250 μm) was coated with clay minerals for further investigations with reactive solutes. The mass of clay per mass of matrix was 0.66% (Fesch et al., 1998). The sand column was saturated from bottom to top with a 10-mM solution of potassium chloride. Due to entrapped air the water saturation was

Table 1
Sand column properties

Column volume	1257 cm^3
Sand mass	2195 g
Particle density	2.65 g cm^{-3}
Porosity, ϕ	0.341 cm^3 cm^{-3}
'Satiated' water content, θ_u	0.263*, 0.268 cm^3 cm^{-3}
Reachable saturation degree, θ_u / ϕ	0.77*, 0.78
Residual water content, θ_r	0.02 cm^3 cm^{-3}
Hydraulic conductivity of sand under 'satiated' conditions, $K(\theta_u)$	0.30*, 0.33 cm min^{-1}
Saturated hydraulic conductivity of the glass plate K_s	0.032*, 0.017 cm min^{-1}
Height of tensiometers above porous plate	5, 19 and 37 cm
Height of TDR probes above porous plate	7, 17, 25, 30, 35, 43 and 53 cm

The marked values (*) were valid after a drying period of 4 months.

78%. The corresponding water content (26.8 cm^3 cm^{-3}) was called 'satiated' (Mualem and Miller, 1979). A resaturation after a drying period of four months resulted in a saturation of 77%. The residual water content was 0.02 cm^3 cm^{-3} as determined in independent experiments.

A porous glass plate 0.55 cm in height and an air entry value greater than 80 cm was placed at the bottom of the column to prevent air invasion through the bottom. The outlet of the column was connected with a tube to a water reservoir. This reservoir was placed on a table that could move up or down at a constant velocity.

The height of the water level in the reservoir controlled the pressure at the porous plate. In a static equilibrium it corresponds with the free water table inside the column. The periodic movement of the reservoir yielded a triangular wave function for the pressure head at the bottom of the column. The pressure and water content were measured by means of three tensiometers and seven time domain reflectometry (TDR) probes, respectively (Fig. 2). Tensiometers (1.5 cm in length, 0.7 cm in diameter) were equipped with pressure transducers (PR-9, Keller, Winterthur) for continuous monitoring (Workbench, Strawberry Tree, USA). TDR probes (three parallel rods, 5.4 cm in length, 0.2 cm in diameter, 0.8 cm spacing) were calibrated with a data logger system (CASMI, Poland). The water content was calculated by comparing the measured signal corrected for offset length and temperature with the offset corrected signal measured in a pure solution (Roth et al., 1990). The calibration of the TDR probes was conducted using small cells (5 cm in diameter, 2 cm in height), filled with the same sand mixture and saturated with the same solution as described above. The cells were drained by lowering the matric potential head stepwise from 0 to −160 cm. After each step TDR signals were recorded and the volumetric water content was determined by monitoring the weight of the system.

The water retention curve was determined in the column for quasi-static pressure conditions using the water-content measurements made in the vicinity of each tensiometer. An averaged pair of main drying and wetting curve was constructed using this data (Fig. 3). The shapes of these curves were not as smooth as the water-retention curves gained from a single TDR probe but they allowed a better description of the overall wetting and drying behaviour of the entire column. Because of the long time periods
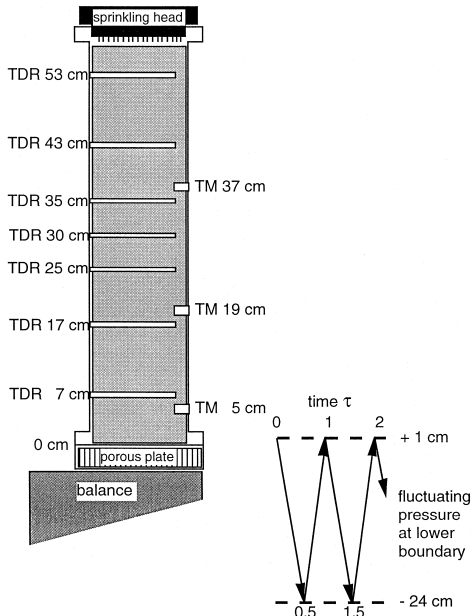
Fig. 2. Experimental set-up.

required to reach water contents close to the residual water content in the upper part of the column, less data were available for describing the wetting curve. The height of the capillary fringe, the 'satiated' zone above the water table, was about 24.5 cm in the drying case and 13.6 cm in the wetting case.
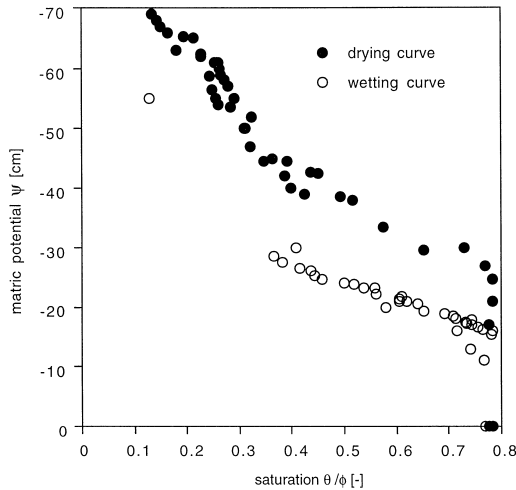

Fig. 3. Measured water-retention curve. The difference between drying and wetting curve is caused by hysteresis. This curve consists of points measured with TDR probes at different elevations.

The hydraulic conductivity of the column under 'satiated' conditions was measured using the steady state head control method (Klute and Dirksen, 1986). The measured conductivity was 0.29 and 0.28 cm min^{-1} for the saturation degree of 78% and 77%, respectively. The hydraulic conductivity of the porous plate was measured with the falling head method (Jury et al., 1991). During the first experiments, clay particles clogged some pores of the porous plate and thus decreased the conductivity. Before the second experimental series the porous plate was cleaned and the saturated conductivity increased again from 0.017 cm min^{-1} to 0.032 cm min^{-1}. The conductivity of the sand itself was calculated from the conductivity of the porous plate and the total conductivity of the column. The value at the 'satiated' state was 0.33 and 0.30 cm min^{-1} for 78% and 77% saturation, respectively.

At the top of the column a sprinkling system was installed. An irrigation head with 20 needles (20 mm long, 0.07 cm diameter) was connected to a stroke pump (RS P 1.8, Hausmann Pumpe, Schlieren, CH) to ensure a homogeneous constant influx at the upper boundary.

3.2. Initial and boundary conditions

In several experiments the influence of different initial and boundary conditions was investigated (Table 2). Before each experiment the column was 'satiated'. The height of the outflow tube was subsequently lowered to the level of 1 cm above the porous plate. Then the tube was connected with the water reservoir to ensure that after an equilibration period the free water table in the column had the same height as the water level in the reservoir. All experiments were started on the boundary drying curve after an equilibration period ranging from several hours to 3 days, depending on the pressure or matric potential applied at the porous plate. After this equilibration period the water level in the reservoir was continuously moved up and down causing pressure variations at the porous plate.

Table 2
Experimental conditions

Upper boundary condition: Flux boundary condition	Flux density (cm min^{-1})
with irrigation	0.06
without irrigation	0.00

Lower boundary condition: Fluctuating pressure boundary	Velocity of water reservoir (cm min^{-1})
fast	1.52
slow	0.28

Initial condition: Pressure at lower boundary	Initial pressure head (cm)
high	+1
low	−24

For some experiments the fluctuations of the water level in the reservoir on the moving plate began 1 cm above the porous plate moving downwards to 24 cm below the plate and rose again to 1 cm above the plate, with at least three cycles per experiment. In other experiments the water level in the reservoir was first slowly lowered to 24 cm below the porous plate and the fluctuations initiated with a wetting process from this level after a second equilibration period.

The applied pressure head at the column bottom thus fluctuated between $+1$ cm to -24 cm, which was expected to induce significant water content changes inside the column, ranging from the 'satiated' state above the porous plate to small water contents near the top of the column. The applied pressure difference of 25 cm was nearly identical to the height of the capillary fringe of the main drying curve.

The velocity of the movement of the water reservoir was 0.28 cm min^{-1} in the slow experiments and 1.52 cm min^{-1} in the fast experiments corresponding to periods of 180 min and 33 min, respectively. The ratio between the velocity of the reservoir and the hydraulic conductivity of the sand at the 'satiated' water content was 1 in the slow case and 5 in the fast case. To compare experiments with different velocities, the time t is expressed as a dimensionless number of cycles $\tau = t/\text{period}$ and the time at the beginning of the fluctuation with the pressure head of $+1$ cm was chosen as time origin τ_0 (Fig. 2).

In one set of experiments the column was irrigated from the top while concurrently raising and lowering the water reservoir. The irrigation and the pressure fluctuations of the lower boundary started simultaneously. The applied irrigation rate was 1 cm^3 min^{-1} (0.06 cm min^{-1}). Therefore two dynamic features, the irrigation and the water table fluctuations, were superimposed.

4. Results and discussion

4.1. Experiments

We measured the influence of different boundary and initial conditions on the water storage in the column, the matric potential head and the water content at given soil depths. In Figs. 4 and 5 two experiments conducted at high velocity (1.52 cm min^{-1}) are compared for different initial conditions. Experiment 1 started with a drying process by lowering the water level from $+1$ to -24 cm while experiment 2 started with a wetting process raising the reservoir from -24 cm to $+1$ cm. In Fig. 4 the results are expressed as average water content, defined as the ratio between total water volume and column volume. The average water content fluctuates about different mean values and it is not obvious if the two values approach each other. While the tensiometer 19 cm above the porous plate showed exactly the same pressure fluctuations in both experiments, the TDR probe at 17 cm registered higher water contents in the experiment which began with a drying cycle (Fig. 5a,b) demonstrating the hysteresis effect of the sandy soil. Above the capillary fringe the fluctuations of the matric potential head at 37 cm and of the water content at 43 cm were very small. The curves seemed to approach slowly a constant value (Fig. 5a).
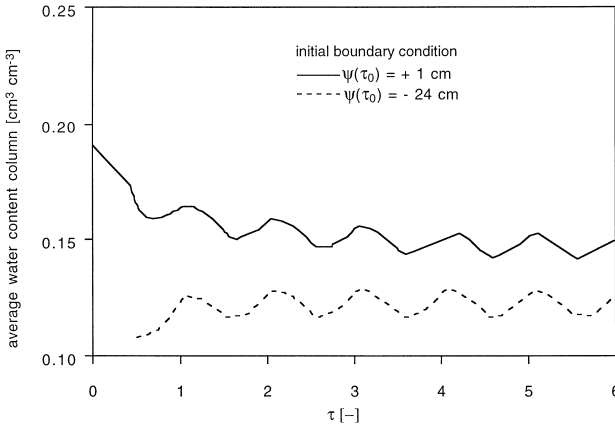
Fig. 4. Influence of different initial conditions at the lower boundary on the water storage in the column expressed as average water content.

The influence of the velocity of the water reservoir movement is shown in Figs. 6 and 7. Both experiments started from an equilibration period in a state with the water level 1 cm above the porous plate. The average water content in the column and the matric potential at the height of 37 cm varied more in the case of slow fluctuations (Figs. 6 and 7a) because the system had more time to respond to the pressure fluctuations at the lower boundary. The matric potential curves of the tensiometer 19 cm above the porous plate oscillated around the same mean value but the amplitude was smaller in the case of rapid fluctuations (Fig. 7a).

The water content at 17 cm was smaller in the fast case although the matric potential values were quite similar (Fig. 7a and b). These differences may be caused by velocity-dependent wetting and drying processes (Blunt and Scher, 1995). However, to explain these differences, more experiments at intermediate velocities need to be carried out. The missing values in Fig. 7b are due to technical difficulties of the TDR system.
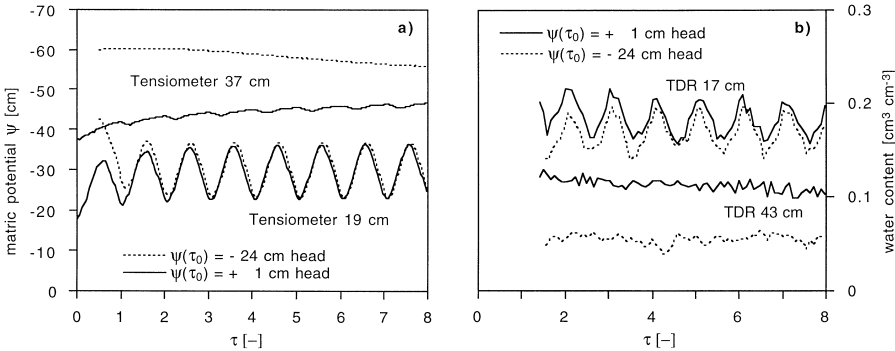

Fig. 5. Influence of different initial conditions at the lower boundary on (a) matric potential and (b) water content above and within the reach of the capillary fringe.
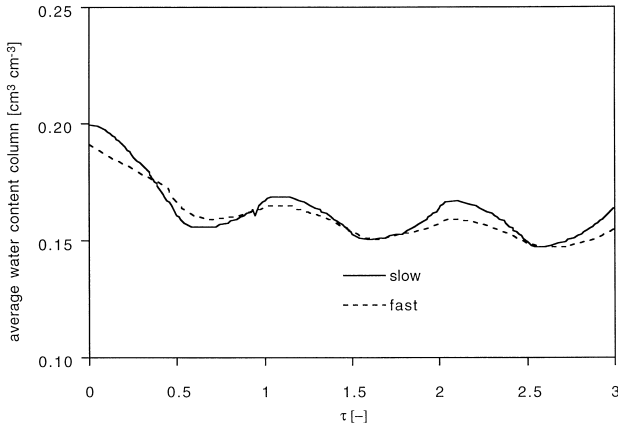
Fig. 6. Influence of different pressure fluctuation velocities imposed at the lower boundary on the water storage in the column expressed as average water content.

While the first series of experiments was carried out with zero flux at the upper boundary, the second set was performed with a downward water flux of 0.06 cm min^{-1}. This flux rate corresponds to 20% of the hydraulic conductivity under 'satiated' conditions. Note that the irrigation and water table fluctuations started simultaneously. So the system responds to a step change of the upper boundary and a periodic fluctuation at the lower boundary. The results are compared with the experiment without irrigation in Figs. 8 and 9. Both experiments started with an equilibration period with the water reservoir level 1 cm above the porous plate. The amplitudes of average water content were similar in both cases but the absolute values were higher in the experiment with irrigation (Fig. 8). As expected also the tensiometer readings showed lower suction in the experiment with irrigation (Fig. 9a). Once in each period, when the water level was 24 cm below the porous plate and the matric potential reached the lowest value, the tensiometer curves approached each other in the irrigated case indicating unit gradient
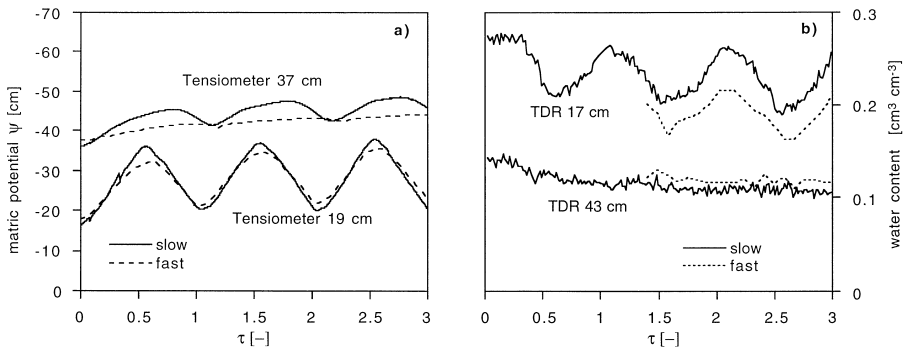
Fig. 7. Influence of different pressure fluctuation velocities imposed at the lower boundary on (a) matric potential and (b) water content above and within the reach of the capillary fringe.
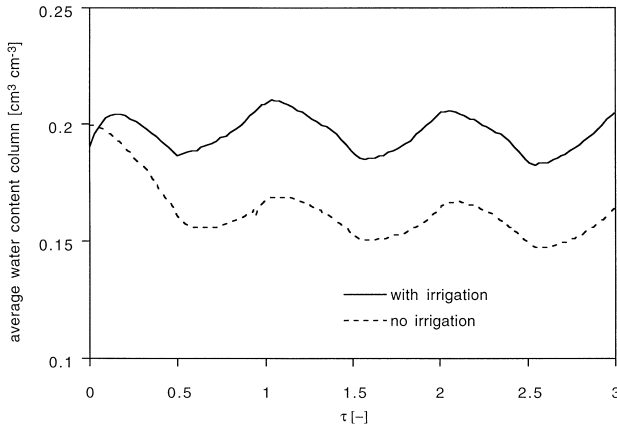
Fig. 8. Influence of different upper boundary conditions on the water storage in the column expressed as average water content.

conditions above the capillary fringe. The TDR probe 17 cm above the porous plate became immersed in the capillary fringe during each fluctuation in the irrigated column while the capillary fringe barely touched this sensor after each period in the case of zero infiltration (Fig. 9b).

4.2. Simulations

Several experiments were compared with simulations carried out with the model HYSTFLOW (Stauffer, 1996). This computer code numerically solves the Richards equation taking into account the hysteretic water retention curve $\theta(\psi)$ and water capacity function $C_W(\psi)$ according to the modified Mualem model (Mualem, 1984).

The Brooks and Corey hydraulic functions (Eqs. (3) and (4)) were used to describe the hydraulic conductivity and the boundary drying and wetting curves. The estimated parameters of the hydraulic functions used for the simulations are listed in Table 3. The
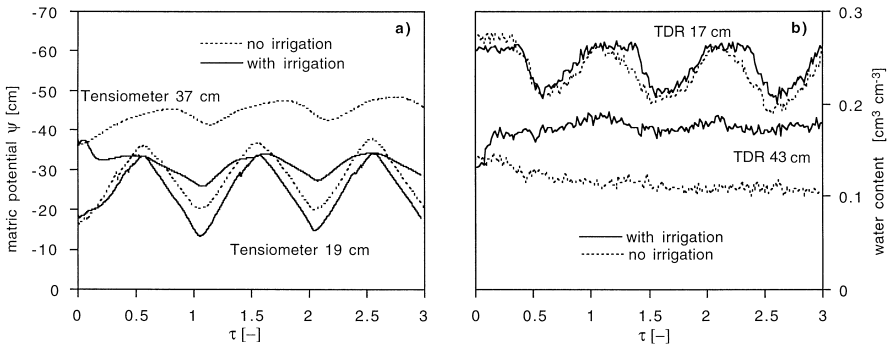

Fig. 9. Influence of different upper boundary conditions on (a) matric potential and (b) water content.

Table 3
Model parameters of the hydraulic functions of the coarse sand

Height of capillary fringe: main drying curve	24.5 cm
Main wetting curve	13.6 cm
Water retention curve: Brooks and Corey shape parameter, λ	1.85
Hydraulic conductivity under completely saturated conditions	0.98 cm min^{-1}
Relative conductivity curve: Brooks and Corey shape parameter, $3+(2/\lambda)$	4.08

column was modeled as a two-material system with the porous plate at the bottom and the sand above. The beginning of the first fluctuation with the water reservoir level at 1 cm above the plate was chosen as the origin of the time axis in the figures. However the preceding saturation of the column and the lowering of the water level from the top of the column down to the initial state at the beginning of the experiment was also simulated as well. The first simulation describes the experiment that started with the water level 1 cm above the porous plate, followed by three cycles of water table fluctuation at the slow velocity (0.28 cm min^{-1}). Subsequently, the water level was decreased to 24 cm below the porous plate and remained there for 12 h. Then the water level fluctuated again for two periods starting at 24 cm below the plate. In Fig. 10 simulations and measurements of the average water content in the column are compared. The simulated initial water content was not identical with the measured one which is caused by an underestimation of drained water volume in the preceding drying of the saturated column. We attribute this difference to the uncertainty of the water-retention curve as determined as a composite of different TDR measurements. To obtain perfect mass balance, more than seven TDR probes should be installed. However, the simulation with a calculated water-retention curve based on the initial value yielded also to similar model behavior.
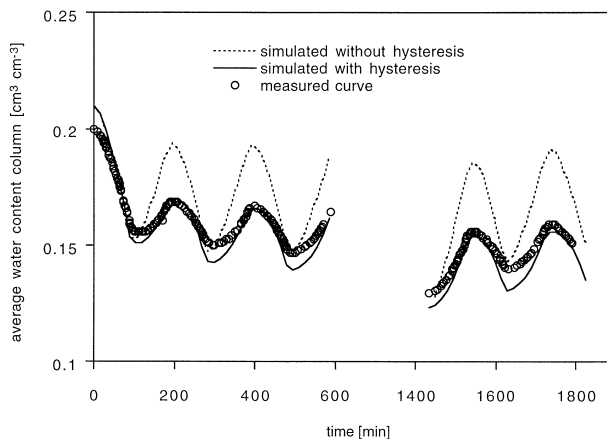

Fig. 10. Experiment without irrigation. Comparison between measured (points) and simulated (lines) water storage in the column expressed as average water content. The simulation was conducted with hysteresis (solid lines) and without hysteresis (dashed lines).

To investigate the influence of hysteresis on average water-content variations, simulations were performed using also nonhysteretic water-retention curves. In Fig. 10 the simulation with the main drying curve is shown as nonhysteretic case. The simulation that accounts for hysteresis describes the measured values better than the simulation without hysteresis. At different elevations above the porous plate simulation results of the nonhysteretic Richards equation exhibited the same behavior as the results for the average water content on the whole column: The amplitude of the water content variations is always overestimated (data not shown).

In Figs. 11 and 12, the measured tensiometer and TDR values are compared with simulations taking into account the hysteresis effect. The simulated values were close to the measured values near and within the capillary fringe but the amplitude of the matric potential values are overestimated in the zone above. The oscillations of the tensiometer measurements were dampened, time delayed and showed a more asymmetrical fluctuation amplitude compared with the simulated curve. The TDR probe at 7 cm height remained immersed in the 'satiated' capillary fringe while the simulation predicts a slight desaturation for the short period when the water level was at its lowest point (-24 cm). The system responds more slowly than predicted with the model. Only the TDR probe at 17 cm above the plate showed high fluctuations while at 30 cm the oscillations practically vanished (Fig. 12). Therefore only the zone just above the capillary fringe contributed to the fluctuations of the average water content. Again, the simulated fluctuation amplitude is slightly overestimated.

While the simulations for the tensiometer readings in or near the capillary fringe supports the validity of the Richards equation, the water content at higher elevations was less accurately described. Noncontinuous air pressure in the capillary fringe seems not to dominate pressure and water transport. The hysteresis and the hydraulic functions under unsaturated conditions are more crucial for the understanding of the water flow in this system.
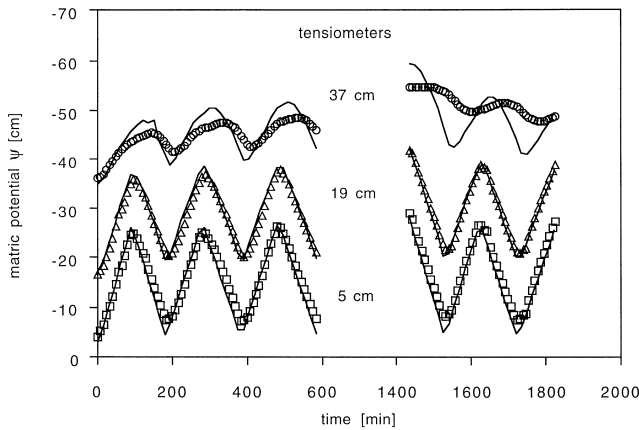

Fig. 11. Experiment without irrigation. Comparison between measured (points) and simulated (solid lines) matric potential head at three elevations.
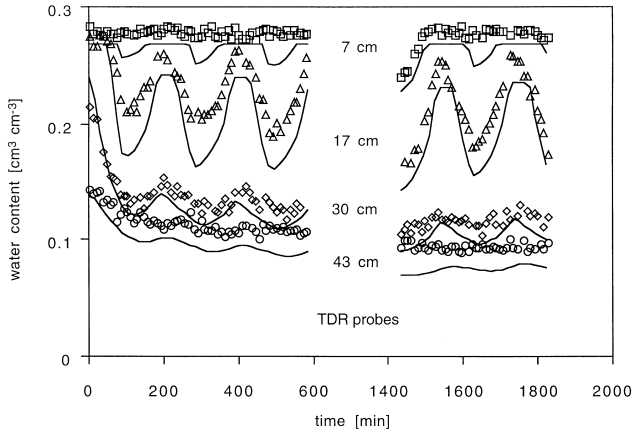
Fig. 12. Experiment without irrigation. Comparison between measured (points) and simulated (solid lines) water content at four elevations.

Next we focus on the simulations of the experiments with irrigation and a fluctuating lower boundary condition. At the beginning the water level was again 1 cm above the porous plate. Taking into account hysteresis, matric potential and water content at given heights were successfully simulated (Figs. 13 and 14). Once in each period the simulated matric potential values 37 cm above the porous plate nearly approached the values of the tensiometer at 19 cm height in agree with the measurements (Fig. 13). The TDR probe 7 cm above the porous plate remained immersed in the capillary fringe for the measured as well as for the simulated case. The water content in the zone between 30 and 43 cm showed nearly constant water contents throughout the whole experiment. This effect was also reproduced by the simulations (Fig. 14).
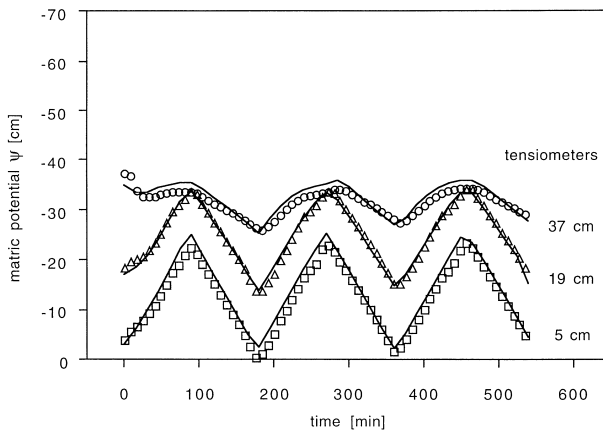

Fig. 13. Experiment with irrigation. Comparison between measured (points) and simulated (solid lines) matric potential head at three elevations.
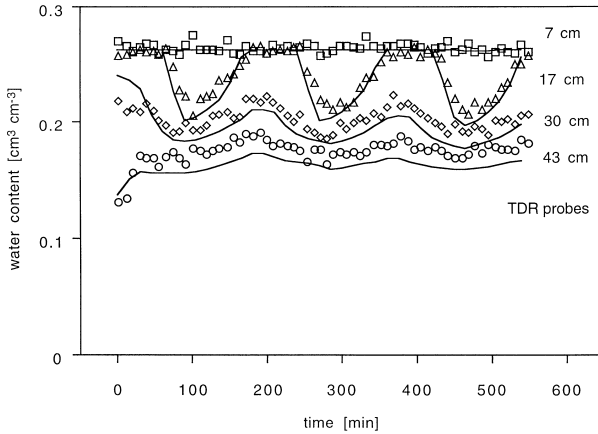
Fig. 14. Experiment with irrigation. Comparison between measured (points) and simulated (solid lines) water content at four elevations.

With respect to the goal of this multidisciplinary project it is important to discuss the implications of the results for the topic of transport of organic pollutants in unsaturated soils. Hysteresis dampens the fluctuations of soil water content due to changing boundary conditions. Complementary to increasing water content, the air content inside the soil column decreases. Aeration and redox potential in hysteretic media may oscillate less than expected if hysteresis is neglected. This may influence the microbial ecology and therefore the degradation of organic pollutants (Sinke et al., 1998). In addition, mixing of dissolved organic pollutants in the soil is probably affected by soil water hysteresis. When a local plume of dissolved organic pollutants resides near the capillary fringe, it may be vertically dispersed by the action of a fluctuating water table. Since hydrodynamic dispersion is dominated by the local velocity field, we expect that this effect is reduced by hysteresis. To determine this influence, the flow itself should be measured inside a column and compared with simulation. Finally, even quite small amounts of dissolved organic pollutants may change the dynamic viscosity of the aqueous phase and the water wettability of the matrix (Dury et al., 1998; Ustohal et al., 1998) causing different hydraulic functions.

5. Conclusions

The water dynamics in a sand column with fluctuating capillary fringe were investigated for different flux and pressure boundary conditions. The dynamics were influenced by the hysteresis of the water retention curve. Depending on the wetting and drying history of the sand, the same matric potential fluctuations caused different water content variations. When the velocity of the pressure oscillations at the lower boundary was increased, the water content near the capillary fringe was lower even with the same preceding history and identical matric potential values.

The average water content of the whole column was dominated by the fluctuations of the water content near the capillary fringe. While tensiometer and TDR measurements showed high fluctuations near the capillary fringe, the oscillations were dampened in higher zones because of reduced hydraulic conductivity. In experiments with high velocity (1.52 cm min^{-1}) this higher zone did not exhibit any fluctuations but gradually approached a new equilibrium state.

The fluctuations of the average water content were dampened and showed an asymmetrical shape due to hysteresis, while the simulation without hysteresis predicts much higher fluctuations and a more symmetrical shape.

The computer code HYSTFLOW (Stauffer, 1996) described the water content and matric potential fluctuations fairly well. But under highly unsaturated conditions the simulations appear to underestimate the dampening effects.

These deviations may be attributed to local heterogeneities, to inaccurately determined hydraulic properties at low matric potential values, or to uncertainties of measuring the water content with short TDR probes. To investigate the hysteresis phenomenon and corresponding numerical models in more detail, the same experiments could be carried out with shorter columns to determine the water-retention curve more accurately. It would also be easier in small columns to measure the hydraulic conductivity under unsaturated conditions to examine the validity of the Brooks and Corey model. Another approach would be the inverse modeling of the water flow to obtain appropriate parameters of the hydraulic functions. However, in the case of coarse sand used in this study, the simulation based on the measured averaged water-retention curve and on the simplified dependent-domain hysteresis model succeeded in predicting general features of the oscillating water distribution.

Acknowledgements

References

Blunt, M.J., Scher, H., 1995. Pore-level modeling of wetting. Phys. Rev. E 52, 6387–6403.

Brooks, R.H., Corey, A.T., 1966. Properties of porous media affecting fluid flow. J. Irrigation Drainage Division, ASCE 92 (IR2), 61–88.

Durner, W., Flühler, H., 1996. Multi-domain model for pore-size dependent transport of solutes in soils. Geoderma 70, 281–297.

Dury, O., Fischer, U., Schulin, R., 1998. Dependence of hydraulic and pneumatic characteristics of soils on a dissolved organic compound. J. Contam. Hydrol. 33, 39–57.

Enderby, J.A., 1955. The domain model of hysteresis: 1. Independent domains. Trans. Faraday Soc. 51, 835–848.

Fesch, C., Lehmann, P., Hinz, C., Haderlein, S.B., Schwarzenbach, R.P., Flühler, H., 1998. Effect of water content on solute transport in a porous medium containing reactive micro-aggregates. J. Contam. Hydrol. 33, 211–230.

Haines, W., 1930. Studies in the physical properties of soil: V. The hysteresis effect in capillary properties, and the modes of moisture distribution associated therewith. J. Agric. Sci. 20, 97–116.

Hillel, D., 1980. Fundamentals of Soil Physics. Academic Press, New York, 413 pp.

Hinz, C., 1998. Analysis of unsaturated/saturated water flow near a fluctuating water table. J. Contam. Hydrol. 33, 59–80.

Hoa, N.T., Gaudu, R., Thirriot, C., 1977. Influence of the hysteresis effect on transient flows in saturated–unsaturated porous media. Water Resour. Res. 13 (6), 992–996.

Jaynes, D.B., 1992. Estimating hysteresis in the soil water retention function. In: van Genuchten, M.Th., Leij, F.J., Lund, L.J. (Eds.), Proceedings of the International Workshop on Indirect Methods for Estimating the Hydraulic Properties of Unsaturated Soils. University of California, Riverside, CA, pp. 219–232.

Jury, W.A., Gardner, W.R., Gardner, W.H., 1991. Soil Physics. Wiley, New York, 328 pp.

Klute, A., Dirksen, C., 1986. Hydraulic conductivity and diffusivity: laboratory methods. In: Klute, A. (Ed.), Methods of Soil Analysis, Part 1, Physical and Mineralogical Methods. American Society of Agronomy, Soil Science Society of America (publisher), Madison, WI, pp. 687–734.

Kool, J.B., Parker, J.C., 1987. Development and evaluation of closed-form expressions for hysteretic soil hydraulic properties. Water Resour. Res. 23 (1), 105–114.

Mualem, Y., 1973. Modified approach to capillary hysteresis based on a similarity hypothesis. Water Resour. Res. 9 (5), 1324–1331.

Mualem, Y., 1974. A conceptual model of hysteresis. Water Resour. Res. 10 (3), 514–520.

Mualem, Y., 1977. Extension of the similarity hypothesis used for modeling the soil water characteristics. Water Resour. Res. 13 (4), 773–780.

Mualem, Y., 1984. A modified dependent-domain theory of hysteresis. Soil Sci. 137 (5), 283–291.

Mualem, Y., Dagan, G., 1975. A dependent domain model of capillary hysteresis. Water Resour. Res. 11 (3), 452–460.

Mualem, Y., Miller, E.E., 1979. A hysteresis model based on an explicit domain-dependence function. Soil Sci. Soc. Am. J. 43, 1067–1073.

Philip, J.R., 1964. Similarity hypothesis for capillary hysteresis in porous materials. J. Geophys. Res. 69 (8), 1553–1562.

Poulovassilis, A., Childs, E.C., 1971. The hysteresis of pore water: The non-independence of domains. Soil Sci. 112, 301–312.

Raats, P.A.C., Gardner, W.R., 1974. Movement of water in the unsaturated zone near a water table. In: van Schilfgaarde, J. (Ed.), Drainage for Agriculture. Agronomy Series, 17, Am. Soc. Agron., WI, pp. 311–357 and 401–405.

Reeves, P.C., Celia, M.A., 1996. A functional relationship between capillary pressure, saturation, and interfacial area as revealed by a pore-scale network model. Water Resour. Res. 32 (8), 2345–2358.

Roth, K., Schulin, R., Flühler, H., Attinger, W., 1990. Calibration of time domain reflectometry for water content measurement using a composite dielectric approach. Water Resour. Res. 26 (10), 2267–2273.

Russo, D., Jury, W.A., Butters, G.L., 1989. Numerical analysis of solute transport during transient irrigation: 1. The effect of hysteresis and profile heterogeneity. Water Resour. Res. 25 (10), 2109–2118.

Sinke, A., Dury, O., Zobrist, J., 1998. Effects of a fluctuating water table: column study on redox dynamics and fate of some organic pollutants. J. Contam. Hydrol. 33, 231–246.

Stauffer, F., 1996. Hysteretic unsaturated flow modelling. In: Proceedings of the Second International Conference on Hydroinformatics, Hydroinformatics '96, Zürich, Switzerland. Balkema, Rotterdam, pp. 589–595.

Sugita, F., Gillham, R.W., 1995a. Pore scale variation in retardation factor as a cause of nonideal reactive breakthrough curves: 1. Conceptual model and its evaluation. Water Resour. Res. 31 (1), 103–112.

Sugita, F., Gillham, R.W., 1995b. Pore scale variation in retardation factor as a cause of nonideal reactive breakthrough curves: 3. Column investigations. Water Resour. Res. 31 (1), 121–128.

Sugita, F., Gillham, R.W., Mase, C., 1995. Pore scale variation in retardation factor as a cause of nonideal reactive breakthrough curves: 2. Pore network analysis. Water Resour. Res. 31 (1), 113–119.

Topp, G.C., 1971. Soil–water hysteresis: the domain theory extended to pore interaction conditions. Soil. Sci. Soc. Am. Proc. 35, 219–225.

Ustohal, P., Stauffer, F., Dracos, T., 1998. Measurement and modelling of hydraulic characteristics of unsaturated porous media with mixed wettability. J. Contam. Hydrol. 33, 5–37.